Impact of Andreev Bound States within the Leads of a Quantum Dot Josephson Junction

Bordin, Alberto; Bennebroek Evertsz, Florian J.; Steffensen, Gorm O.; Dvir, Tom; Mazur, Grzegorz P.; Van Driel, David; Van Loo, Nick; Wolff, Jan Cornelis; Kouwenhoven, Leo P.; More Authors

DOI
10.1103/PhysRevX.15.011046

Publication date
2025

Document Version
Final published version

Published in
Physical Review X

Impact of Andreev Bound States within the Leads of a Quantum Dot Josephson Junction

Alberto Bordin,[1,*] Florian J. Bennebroek Evertsz',[1,*] Gorm O. Steffensen,[2,3,4,*] Tom Dvir,[1,†] Grzegorz P. Mazur,[1] David van Driel,[1] Nick van Loo,[1] Jan Cornelis Wolff,[1] Erik P. A. M. Bakkers,[5] Alfredo Levy Yeyati,[2,3,6] and Leo P. Kouwenhoven[1,‡]

[1]*QuTech and Kavli Institute of NanoScience, Delft University of Technology, Delft, The Netherlands*
[2]*Departamento de Física Teórica de la Materia Condensada, Universidad Autónoma de Madrid, Madrid, Spain*
[3]*Condensed Matter Physics Center (IFIMAC), Universidad Autónoma de Madrid, Madrid, Spain*
[4]*Instituto de Ciencia de Materiales de Madrid (ICMM), Consejo Superior de Investigaciones Científicas (CSIC), Sor Juana Inés de la Cruz 3, 28049 Madrid, Spain*
[5]*Department of Applied Physics, Eindhoven University of Technology, Eindhoven, The Netherlands*
[6]*Instituto Nicolás Cabrera, Universidad Autónoma de Madrid, Madrid, Spain*

(Received 28 April 2024; revised 15 October 2024; accepted 6 January 2025; published 3 March 2025)

Detection and control of Andreev bound states (ABSs) localized at semiconductor-superconductor interfaces are essential for their use in quantum applications. Here we investigate the impact of ABSs on the supercurrent through a Josephson junction containing a quantum dot (QD). Additional normal-metal tunneling probes on both sides of the junction unveil the ABSs residing at the semiconductor-superconductor interfaces. Such knowledge provides an ingredient missing in previous studies, improving the connection between theory and experimental data. By varying the ABS energies using electrostatic gates, we show control of the switching current, with the ability to alter it by more than an order of magnitude. Finally, the large degree of ABS tunability allows us to realize a three-site Andreev molecule in which the central QD is screened by both ABSs. This system is studied simultaneously using both supercurrent and spectroscopy.

DOI: 10.1103/PhysRevX.15.011046

Subject Areas: Condensed Matter Physics, Semiconductor Physics, Superconductivity

I. INTRODUCTION

Quantum dots (QDs) confine electrons into orbitals with discrete energies, similar to individual atoms [1]. They find countless applications as sensors [2,3], light sources [4,5], or qubits [6,7]. Superconductors, on the other hand, feature an attractive pairing between electrons, condensing them into a sea of Cooper pairs [8]. One consequence of this pairing is the ability to carry supercurrent: zero-resistance transport of electron pairs. Supercurrent can flow even if two superconducting leads are connected by a thin insulating material or a weak link. Such a system is known as a Josephson junction and forms the core component behind superconducting qubits [9,10] and superconducting diodes [11].

Using semiconducting QDs as weak links in Josephson junctions combines the precise orbital tunability of QDs with the quantum coherent properties of superconductors, resulting in substantial control over the supercurrent [12–16] and facilitating circuit quantum electrodynamics operation [17,18]. Intriguingly, QDs can also hybridize with a superconductor. For example, when hosting an odd number of electrons, a QD acts as a localized spin 1/2, which becomes screened by quasiparticles at stronger coupling, resulting in a spinless Yu-Shiba-Rusinov ground state [19–22]. Control of this interaction allows for tuning of both the ground-state composition and the spectrum; an interesting lever for Andreev spin qubits [23–26], Kitaev chains [27–29], and the creation of larger superconducting molecules [30–35]. However, typical devices are prone to the formation of accidental QDs or localized Andreev bound states (ABSs) due to defects or impurities [36–38]. Such states are hard to characterize and control and are generally detrimental to device operation. Conversely, recent works have shown that gate-controlled ABSs are

[*]These authors contributed equally to this work.
[†]Present address: Quantum Machines, Tel Aviv, Israel.
[‡]Contact author: l.p.kouwenhoven@tudelft.nl

useful for tuning the coupling between sites in minimal Kitaev chains [39–42], spurring further interest in measuring and manipulating them.

In this work, we investigate—theoretically and experimentally—the impact of ABSs on a QD-based Josephson junction and distinguish its features from a S-QD-S junction. We show how gate tuning of ABSs affects both the size and gate symmetries of the critical current—an important quantity, e.g. for Andreev spin qubits, whose readout signal is proportional to it [25,26]. Furthermore, we study the influence of the QD-ABS tunnel coupling on the spin screening of the odd-parity doublet state by comparing measurements of zero-bias conductance and critical current. In this manner, we realize an ABS-QD-ABS Andreev trimer where the screening of the central QD is facilitated by ABSs in both leads, highlighting their potential use in realizing larger chains and artificial molecules.

II. DEVICE

A tunable Josephson junction can be realized by contacting a semiconducting nanowire with two superconducting leads [13,20,21,43]. In this work, two Al contacts are deposited on an InSb nanowire using the shadow-wall lithography technique [44] creating two superconducting-semiconducting hybrid segments [45]. In addition, we introduce one Au normal contact at each end of the device. Below the nanowire, separated by a thin dielectric, an array of bottom gates defines an electrostatic potential along the device, as Fig. 1(a) illustrates. The three gates between the hybrid segments form a QD; its chemical potential is controlled by V_{QD} while the barriers are tuned by V_{TL} and V_{TR}. Two additional outer barriers separate each hybrid from the external normal contacts, turning them into tunneling probes.

The device is loaded in a dilution refrigerator with a base temperature of approximately 15 mK. Both normal contacts are connected to corresponding voltage sources and current meters (V_{L}, I_{L} and V_{R}, I_{R}). The Josephson junction in the middle of our device is connected to a flexible circuit that enables setting either a voltage bias or a current bias across the junction. Figure 1(b) shows that while the left Al contact is always grounded, the right one is connected to a switch between either a voltage source with a current meter (V_{bias}, I_{meas}) or a current source with a voltage meter (I_{bias}, V_{meas}). See Supplemental Material [46] for further nanofabrication and circuit details (Fig. S3).

Figure 1(c) reports a voltage-bias measurement characterizing the QD's Coulomb blockade diamonds. In Fig. 1(d), instead, we apply a current bias and observe a $V_{\mathrm{meas}} = 0$ region, which is identified as the dc supercurrent regime. The transition from zero to finite voltage is marked by a blue line, with the associated current-bias values denoted as I_{sw}, the switching current. An explanation of how I_{sw} is extracted is presented in Fig. S4 of Supplemental Material [46]. As previously demonstrated in the literature,

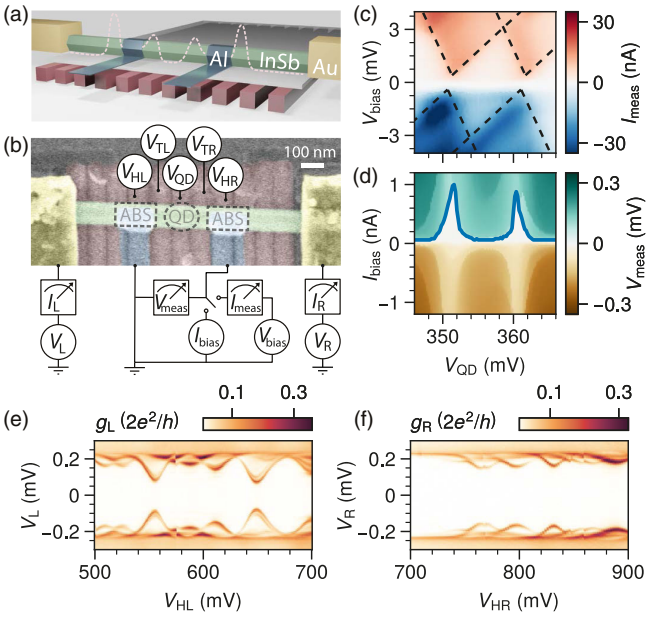

FIG. 1. (a) Illustration of the device. (b) Schematic of the measurement setup on a false-colored scanning electron micrograph of the reported device. (c) I_{meas} as a function of V_{QD} and V_{bias} showing a single Coulomb diamond. The dashed lines correspond to a constant-interaction QD model [6] with charging energy $U = 2.7$ meV, lever arm $\alpha = 0.26$, positive slope $\beta = \alpha/0.7$, and superconducting gap $\Delta = 0.2$ meV. (d) V_{meas} as a function of V_{QD} and I_{bias}. The blue line identifies the switching current I_{sw}, where the Josephson junction transitions from a superconducting to a resistive regime. (e),(f) Examples of typical tunneling spectroscopy measurements (from a previous cooldown of the same device) of the left and right hybrids, respectively; $g_{\mathrm{L}} \equiv (dI_{\mathrm{L}}/dV_{\mathrm{L}})$ and $g_{\mathrm{R}} \equiv (dI_{\mathrm{R}}/dV_{\mathrm{R}})$ are measured with standard lock-in techniques.

$I_{\mathrm{sw}}(V_{\mathrm{QD}})$ depends sensitively on the QD gate voltage. The device behaves like a supercurrent transistor: I_{sw} is maximal at the QD charge degeneracies, where the parity transitions between even and odd, while it is suppressed whenever the QD is off resonance [12,13].

The novelty of our device is highlighted in Figs. 1(e) and 1(f), which show examples of tunneling spectroscopy measurements performed from the left and right normal probes, yielding differential conductance g_{L} and g_{R}, respectively. Both hybrid segments feature ABSs that disperse as a function of the gate voltages V_{HL} and V_{HR}. To understand their implications, we introduce in the following section a minimal three-site model, considering a single ABS on the left, a single QD orbital in the center, and a single ABS on the right.

III. MODEL

The left and right ABSs are modeled as single levels with negligible charging energy ($U_{\mathrm{ABS}} = 0$) coupled to BCS

superconductors by couplings $\Gamma_{L/R}$ in the atomic limit [53]. Both ABSs are tunnel coupled to a central QD with a large charging energy $U \sim 10\Delta$, where Δ represents the energy of the superconducting gap. This system is described by the following Hamiltonian:

$$H = H_{ABS} + H_D + H_T, \tag{1}$$

$$H_{ABS} = \sum_{j=L/R} \left[\xi_j n_j + \Gamma_j d^\dagger_{j\uparrow} d^\dagger_{j\downarrow} + \text{H.c.}\right], \tag{2}$$

$$H_D = \frac{U}{2}(n - n_C)^2, \tag{3}$$

$$H_T = \sum_{j=L/R} \sum_{\sigma=\uparrow/\downarrow} t_j d^\dagger_{C\sigma} d_{j\sigma} + \text{H.c.} \tag{4}$$

Here, $\xi_{L/R}$ are the single-level energies, with $n_{L/R}$ and $d^\dagger_{L/R\sigma}$ denoting the corresponding number and creation operator. These result in ABS excitation energies $E_{L/R} = \sqrt{\xi^2_{L/R} + \Gamma^2_{L/R}}$ and particle-hole coherence factors $u^2_{L/R} = \frac{1}{2}[1 + (\xi_{L/R}/E_{L/R})]$ and $v^2_{L/R} = 1 - u^2_{L/R}$ [53]. The central QD is described by a typical Anderson model with creation operators $d^\dagger_{C\sigma}$, the number operator $n = d^\dagger_{C\uparrow} d_{C\uparrow} + d^\dagger_{C\downarrow} d_{C\downarrow}$, and the number n_C fixing the mean dot population controlled by V_{QD}. Lastly, the QD is tunnel coupled to the ABSs by couplings $t_{L/R} = |t_{L/R}| \exp[i\phi_{L/R}]$, with the phase drop across the junction characterized by the difference $\phi = \phi_L - \phi_R$. A sketch of the model is depicted in Fig. 2(a). This model neglects both the detailed structure of the ABSs, e.g., multiple orbitals, and any screening of the QD due to a direct coupling to the BCS density of states [21,54], capturing only the screening stemming from the coupling to ABSs. Consequently, the validity of the model is limited to where ABSs are tuned close to their energy minima. More details can be found in Supplemental Material [46]. Theory plots in this manuscript are produced with numerical diagonalization of Eq. (1), capturing QD-ABS hybridization and its dependence on $u_{L/R}$, $v_{L/R}$, and n_C, for all coupling regimes. Here, we define the junctions critical current as $I_c = \max_\phi [I(\phi)]$ following typical conventions, which in plots is obtained numerically.

For low ABS-QD coupling, intuition on the behavior of I_c can be obtained from lowest-order (fourth) perturbation theory in $t_{L/R}$. This yields qualitatively similar I_c curves to a weakly coupled QD junction with BCS leads (denoted with the letter S): QD parity transitions ($n_C = 0.5$ or 1.5) result in peaks of I_c accompanied by a switch from a 0 to a π phase [13,55]. However, the supercurrent through an S-QD-S junction involves virtual occupation of the BCS continuum, while the supercurrent through an ABS-QD-ABS junction instead relies on the occupation of the ABSs

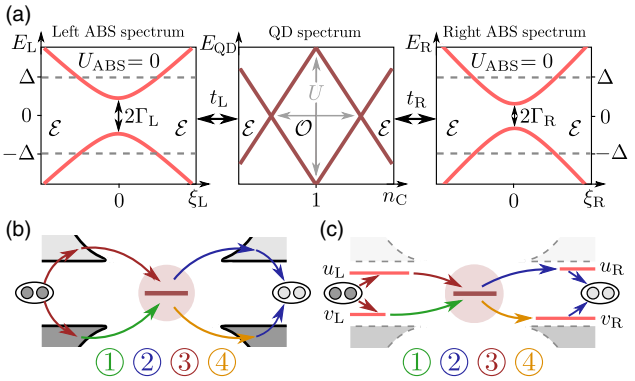

FIG. 2. (a) Schematic of the ABS-QD-ABS model depicting the decoupled ($t_{L/R} = 0$) electronic spectrum of each component. The scale Δ illustrates the position of the BCS continuum neglected in the model, while the QD spectrum is shown in scale of U. Symbols $\mathcal{E}$ and $\mathcal{O}$ indicate even and odd ground-state parity, respectively. Smaller sketches resembling this schematic are used in the following figures to indicate gate settings. (b),(c) Sketches of fourth-order cotunneling contributions to the critical current I_c for an S-QD-S model (b) and an ABS-QD-ABS model (c). The numbers below indicate the ordering of the dominant fourth-order process for an empty QD ($n = 0$).

[Figs. 2(b) and 2(c)]. In the $U \gg \Delta$ limit, the peak I_c is given by

$$I^{\text{S-QD-S}}_{c,\text{peak}} \approx \frac{8e}{\hbar} \frac{|t_L|^2 |t_R|^2}{2\Delta^3} (\Delta\rho_L)(\Delta\rho_R), \tag{5}$$

$$I^{\text{ABS-QD-ABS}}_{c,\text{peak}} \approx \frac{8e}{\hbar} \frac{|t_L|^2 |t_R|^2}{E_L E_R (E_L + E_R)} \left(\frac{\Gamma_L}{2E_L}\right)\left(\frac{\Gamma_R}{2E_R}\right), \tag{6}$$

where $\rho_{L/R}$ denotes the density of states. Here, the factors $(\Delta\rho_{L/R})$ and $(\Gamma_{L/R}/2E_{L/R})$ correspond to $|u_{L/R} v_{L/R}|$, which denote the expectation value of adding or removing a Cooper pair [43]. Intuitively, the ABS energies $E_{L/R}$ act as a gap, and the additional powers of $E_L E_R$ in the denominators stem from the asymmetrical coherence factors when $\xi_{L/R} \neq 0$ [56]. Further details on the calculations, including more terms and the n_C dependence, are reported in Supplemental Material [46].

This perturbative approach highlights the difference between S-QD-S and ABS-QD-ABS junctions and inspires the next section. Since both $E_{L/R}$ and the $u_{L/R}$ and $v_{L/R}$ components depend on $\xi_{L/R}$, tunable by $V_{HL/HR}$, their effect on the supercurrent can be tested experimentally.

IV. SUPERCURRENT CONTROL

To test the impact of ABSs on the supercurrent, we focus in Fig. 3(a) on a single ABS weakly coupled to the QD. In Fig. 3(c), we measure the switching current I_{sw} as a function of V_{QD} at three different positions along V_{HL}, color coded to the vertical line cuts shown in Fig. 3(a).

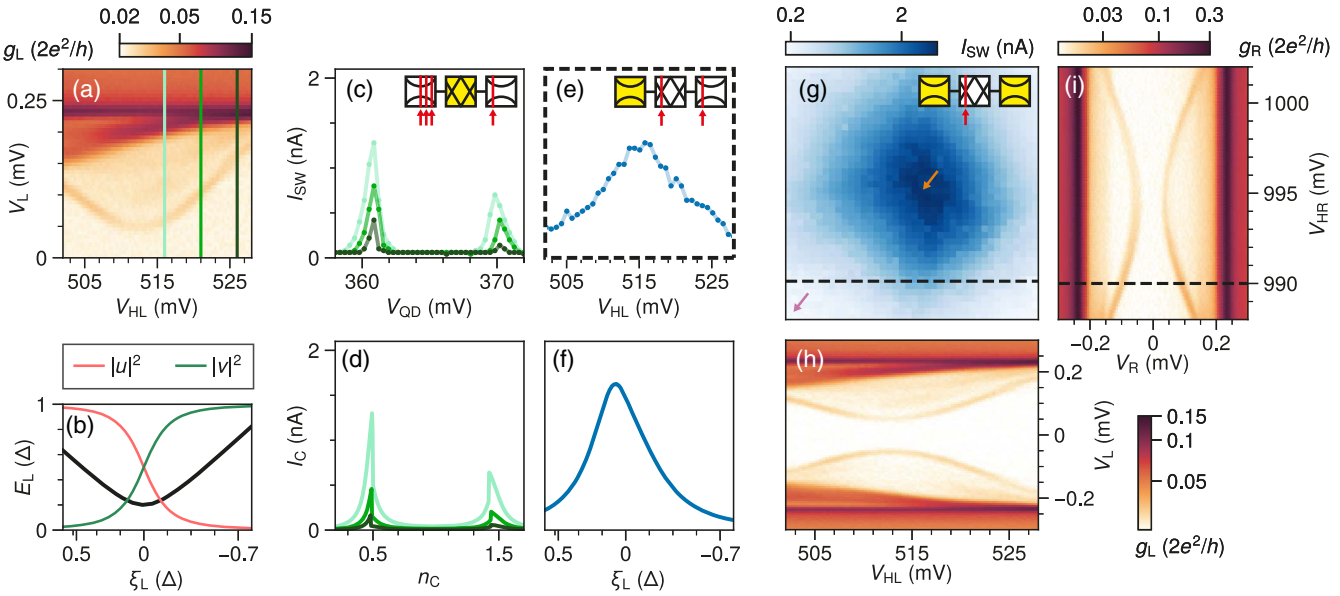

FIG. 3. (a) g_L as a function of V_L and V_{HL}, showing the ABS energy dispersion. (b) ABS energy and square of the particle-hole components u_L and v_L as predicted by the theory model. (c) I_{sw} as a function of V_{QD} ranging over a single QD orbital and color coded to the vertical line cuts in panel (a). The inset illustrates the chemical potentials of the three sites of our system. When a site is colored yellow, the corresponding chemical potential is varied. Otherwise, a red arrow indicates the fixed position of the chemical potential. (d) I_c predicted by the theory model. (e) I_{sw} as a function of V_{HL}, tracing the left QD parity transition in panel (c). (f) Theory I_c as a function of ξ_L, tracing the left QD parity transition in panel (d). (g) I_{sw} as a function of V_{HL} and V_{HR}. $V_{QD} \approx 361$ mV, tracing the left QD parity transition as shown in Fig. S7 of Supplemental Material [46]. The black dashed line indicates the position along V_{HR} at which I_{sw} in panels (c) and (e) is measured. (h),(i) Spectra of both hybrids [panel (h) shows the same data as panel (a) but including negative V_L values]. For both panels, V_{QD} is fixed at 358 mV. All other figures in the manuscript, excluding Figs. 1(e) and 1(f), which were measured in a previous cooldown, make use of the same ABSs shown here.

We observe an overall increase in I_{sw} as we move closer to the minimum energy of the ABS, which is reproduced by the model in Fig. 3(d), and which can be understood from the denominator in Eq. (6). When comparing theory to experiment, we distinguish between measured switching current I_{sw} and theoretical critical current I_c since I_{sw} might be reduced ($I_{sw} < I_c$) by circuit noise and thermal fluctuations [8]. In some instances, the employed minimal model predicts I_c to be smaller than the measured I_{sw}. These discrepancies we ascribe to missing critical current contributions from, e.g., direct coupling to the BCS states or neighboring QD and ABS orbitals neglected in the model. We stress that all parameters of the model, apart from t_L and t_R, are estimated from independent measurements such as ABS spectroscopy and QD Coulomb diamonds (see Fig. S5 in Supplemental Material [46]). The summary of all extracted and fitted model parameters is reported in Supplemental Material [46] (Table 1).

So far, we studied the switching current as a function of V_{QD}. To study it instead as a function of V_{HL}, we may track the I_{sw} peak value along one of the QD parity transitions (as detailed in Supplemental Material [46] Fig. S7c). In Fig. 3(e), we plot I_{sw} (blue) as a function of V_{HL}, tracking the left QD parity transition in Fig. 3(c). We observe a maximum I_{sw} of 1.28 nA around the ABS minimum energy and a decline in I_{sw} as we move away from this minimum. Notably, I_{sw} is decreased as low as 0.24 nA when E_L approaches Δ, suggesting that most of the supercurrent is mediated via the ABS and not via the BCS continuum. This is supported by the model, which does not include these continuum states and yields a similar decrease in Fig. 3(f). Finally, we note in Figs. 3(d) and 3(f) that I_c is not symmetric around $n_C = 1$ and $\xi_L = 0$. This feature is visible with the numerical diagonalization of Eq. (1) and is not captured by fourth-order perturbation theory. We will return to such asymmetries in Fig. S2 in Supplemental Material [46] and in the following section dedicated to stronger couplings (Fig. 4).

Thus far, the ABS in the right hybrid was kept at $V_{HR} = 990$ mV. In Fig. 3(g), we present I_{sw} as a function of both ABS gates. In the corners of Fig. 3(g), both ABSs are tuned away from their energy minima, resulting in a minimal I_{sw} of 0.12 nA (pink arrow). Along the sides of the panel, a single ABS reaches its energy minimum, resulting in an increase of I_{sw} to approximately 1 nA. In the middle of the panel, both ABSs are positioned at their energy minima, resulting in a maximum enhancement of I_{sw} up to 2.58 nA (orange arrow). Controlling the ABSs, we can modulate I_{sw} by over an order of magnitude.

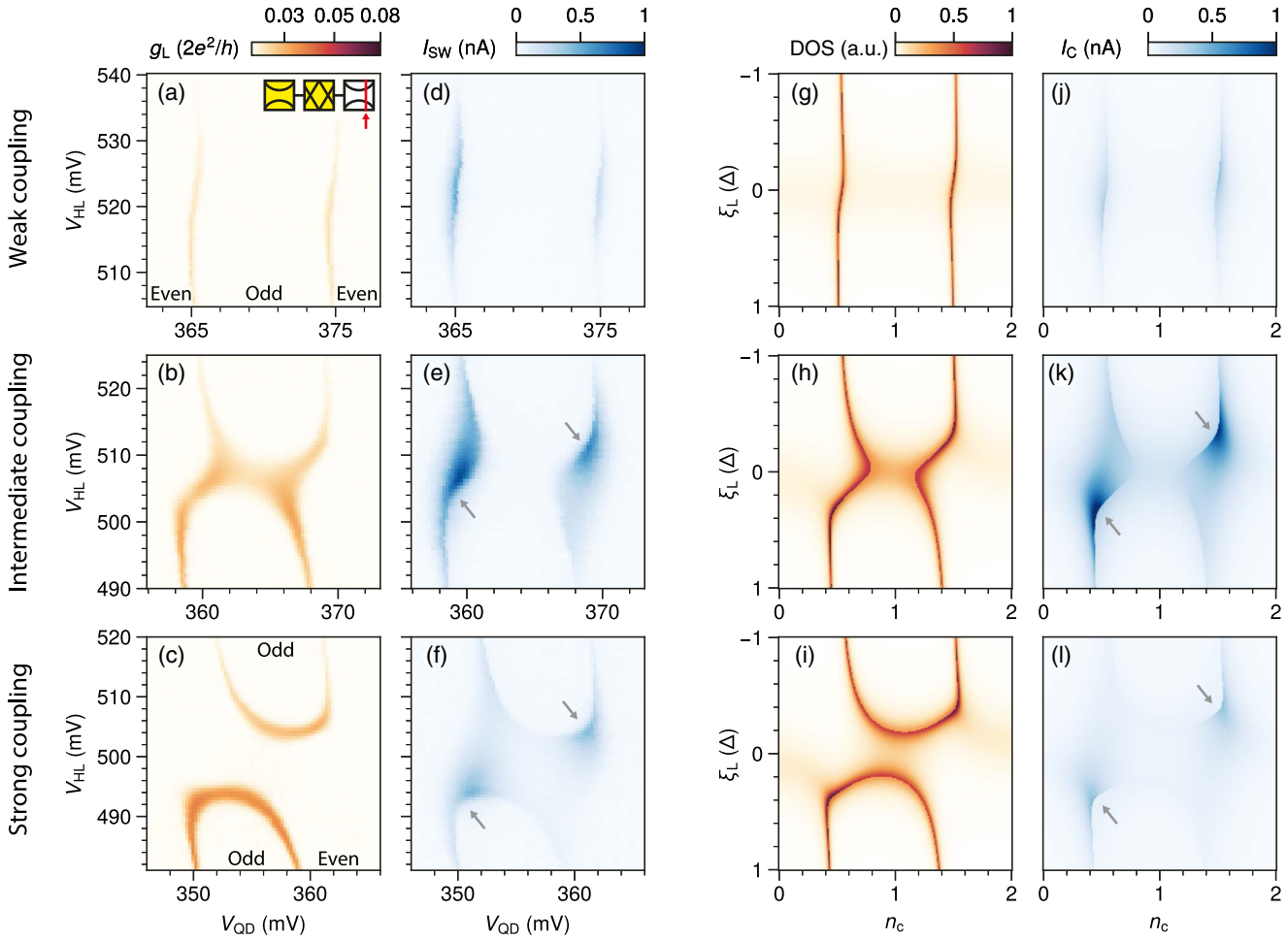

FIG. 4. (a)–(c) Zero-bias conductance g_L as a function of V_{QD} and V_{HL} for weak, intermediate, and strong QD-ABS hybridization. The strength is tuned by the tunnel gate voltage $V_{TL} = 210$, 220, and 226 mV for panels (a), (b), and (c), respectively. The spectrum of the ABSs is reported in Fig. S8 of Supplemental Material [46]. (d)–(f) 2D maps of the switching current corresponding to the same gate range of panels (a)–(c). (g)–(i) Theory simulation of the zero-energy density of states using the Lehmann representation at $\phi = 0$ (see Supplemental Material [46]). (j)–(l) Simulated critical current using our minimal three-site model. Panels (g),(j), (h),(k), and (i),(l) share the same model parameters.

V. ANDREEV TRIMER

After demonstrating switching current control, we turn our attention to the physics of an ABS-QD-ABS molecule. Conceptually, this setup is reminiscent of an S-QD-S junction. However, while the screening states of the S-QD-S junction are of a complicated Kondo-like nature [55,57], the ABS-QD-ABS equivalents are simpler. Here, at odd parity the QD binds to an excited ABS, gaining an exchange energy E_{ex} of order approximately $|t_{L/R}|^2/U$. If E_{ex} exceeds $E_{L/R}$, then the QD odd-parity ground state is screened and rendered into a molecular singlet state of even parity. To investigate this bonding, we fix the electrochemical potential of the right ABS and study the coupling between the left ABS and the QD by looking at the ABS-QD charge stability diagrams of Fig. 4 (the right ABS set points are shown in Fig. S8 of Supplemental Material [46]). Because of our device geometry, charge stability diagrams can be measured either via tunneling spectroscopy from the normal probes or via supercurrent through our Josephson junction. In the first case, the parity transitions of the QD are identified by zero-bias conductance peaks and, in the second case, by switching current peaks.

We can vary the ABS-QD coupling from weak to strong by tuning V_{TL}. The crossover is characterized by a critical tunnel coupling $t_L^c = \sqrt{U\Gamma_L/6}$ (see Supplemental Material [46] for a detailed derivation). When the coupling is weak [$t_L \ll t_L^c$, Figs. 4(a) and 4(d)] the QD parity transitions are barely shifted along V_{QD} as we sweep V_{HL}. As a result, the odd-parity sector separating the even-parity sectors remains roughly equal in width. In the intermediate-coupling case [$t_L \lesssim t_L^c$, Figs. 4(b) and 4(e)], the QD parity transitions are visibly modulated, and the odd-parity sector is reduced as shown in Fig. 4(b). In the strong case [$t_L > t_L^c$, Figs. 4(c) and 4(f)], the topology of the ABS-QD charge stability

diagram is changed [33,58]: When the ABS is at its energy minimum, the system no longer transitions to an odd-parity ground state. All coupling regimes are accurately reproduced by our model in both conductance and supercurrent simulations [Figs. 4(g)–4(l)].

In the weak-coupling regime, the switching current could be understood with fourth-order perturbation theory; the presence of ABSs quantitatively affects I_c, with $E_{L/R}$ mimicking a smaller Δ. However, in the intermediate- and strong-coupling regimes, the presence of ABSs leads to a qualitative difference as well: The gray arrows in Figs. 4(e), 4(f), 4(k), and 4(l) highlight strong asymmetries in the switching current peak heights. Such asymmetries are due to the u and v components of the ABSs. Approaching, e.g., $n_C \sim 0.5$, the ABS-QD hybridization is strongest for an ABS with $|u| \gg |v|$ as then both the ABS and the QD are most easily excited by the addition of an electron. This stronger hybridization results in a higher I_c, as shown also in Fig. S1 of Supplemental Material [46]. Switching current peak asymmetries were previously attributed to multiple QD orbitals [13]. Here we propose an additional possibility for hybrid devices: asymmetries explained by the coherence factors of subgap ABSs.

A. Simultaneous tuning of all three sites

Finally, we turn our attention to the full three-site Andreev molecule by varying the right ABS as well. Figure 5 shows 3D charge stability diagrams extracted from zero-bias conductance measurements (the technique is explained in Fig. S6 of Supplemental Material [46]). In the weak-coupling regime ($t_L \ll t_L^c$, $t_R \ll t_R^c$), the parity transitions form two parallel planes, isolating an odd-parity region between two even-parity regions; here, varying V_{QD} can always switch the ground-state parity, regardless of the ABS tuning, indicating the independence of the three components. In the intermediate-coupling regime ($t_L \lesssim t_L^c$, $t_R \lesssim t_R^c$), the situation is different, as can be appreciated by the different topology of the parity transition manifold, which presents a hole connecting the two even-parity regions. In this regime, it is only when both ABSs are simultaneously at their minimum energy that the odd-parity sector can be screened to an even parity, indicating $E_{ex} > E_{L/R}$, while a single ABS at minimum energy cannot fully screen the odd-parity sector. This shows that the two ABSs can cooperate in the screening of the QD spins, expanding the regions where the system has an even-parity ground state. The even-parity regions expand even further in the strong-coupling regime ($t_L > t_L^c$, $t_R > t_R^c$), where the topology of the parity transition manifold is changed once more. Here, a single ABS positioned at its energy minimum is able to fully screen the odd-parity QD state, as observed by the odd-parity domes being present only in the four corners of the diagram where both ABSs are tuned away from their energy minima.

To appreciate the effect on the supercurrent of the parity transitions shown in Fig. 5, we focus in Fig. 6 on the strong-coupling regime. Keeping the QD gate fixed as in Fig. 6(c), we study the system as a function of both ABS gates. Figure 6(a) shows the measured charge stability diagram, while Fig. 6(b) shows the corresponding I_{sw} map. The theory counterpart is presented in Figs. 6(d) and 6(e). These simulations reproduce the experimental features, apart from a discrepancy between I_{sw} and I_c at the center of Figs. 6(b) and 6(e), where both ABSs are tuned to their energy minima. We speculate that this discrepancy stems from the possibility of ground-state transitions as a function of the phase difference ϕ. If the QD were screened by a single ABS, the odd-parity region would be limited by the black line in Fig. 6(f). With two ABSs at $\phi = 0$, the region shrinks under the blue dashed line, indicating that the ABSs can cooperate to screen the QD. Conversely, at $\phi = \pi$, the region expands to the green dashed line, reflecting competition between the ABSs [59,60]. This phase dependence results in an area in Fig. 6(e) where the ground state transitions from singlet to doublet as ϕ changes from 0 to π. This area is shown with red overlays in Figs. 6(e) and 6(f), and qualitatively matches the area of discrepancy between Figs. 6(b) and 6(e). We recall that our critical current is defined as $I_c = \max_\phi [I(\phi)]$. If the ground state is unstable as a function of the phase, the real device is affected by nontrivial phase dynamics and might switch prematurely to the resistive branch. These phase-induced ground-state

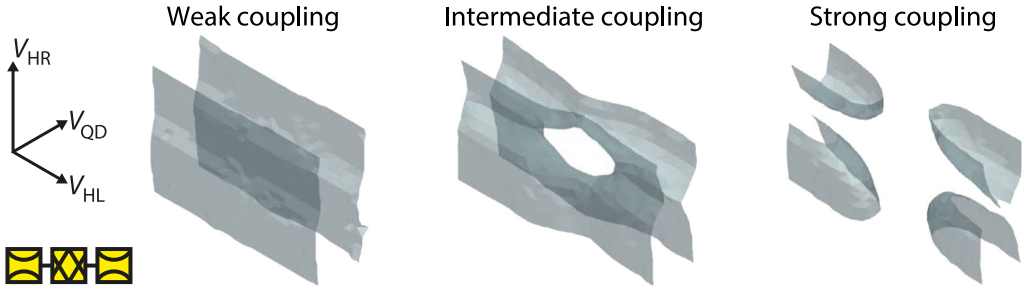

FIG. 5. Measured 3D charge stability diagrams for weak, intermediate, and strong coupling between the QD and the neighboring ABSs. The blue surfaces delineate the boundaries between even and odd parity. See Fig. S6 in Supplemental Material [46] for the measurement details.

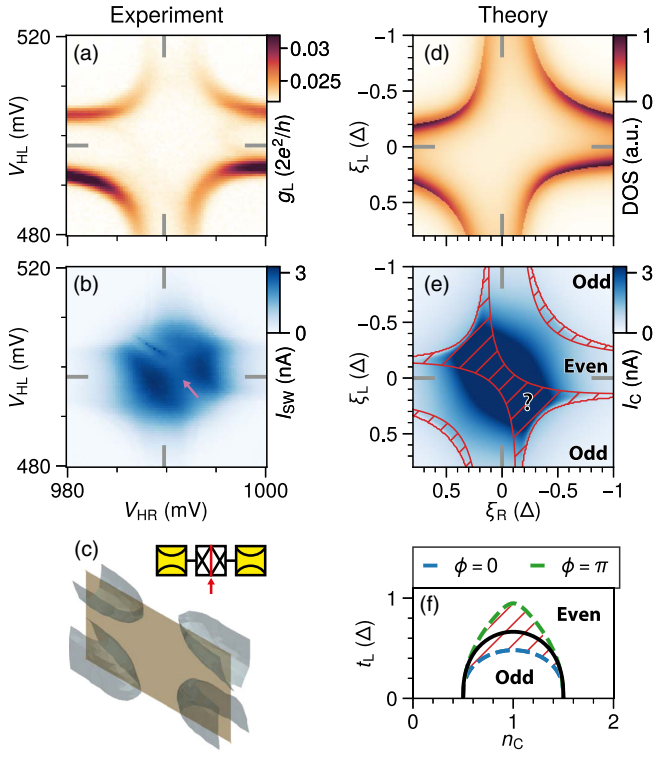

FIG. 6. (a) Left zero-bias conductance g_L as a function of V_{HL} and V_{HR} in the strong-coupling regime. Gray lines indicate the positions of the energy minima of both ABSs. (b) A 2D switching current map. In both panels (a) and (b), V_{QD} is placed between the two QD parity transitions as panel (c) indicates. (d) Theory simulation of the zero-energy density of states using the Lehmann representation at $\phi = 0$. (e) Simulated critical current using our minimal three-site model. Panels (d) and (e) share the same model parameters. (f) A phase-space diagram indicating the ground-state transitions of the system at $\phi = 0$ (blue) and $\phi = \pi$ (green) for parameters of (d) and (e) with $t_L = 0.7$ and $t_R = 0.8$. For comparison, in black the ground-state transitions are illustrated assuming a single ABS. The red-shaded areas of panels (e) and (f) indicate the region where $\phi = 0$ and $\phi = \pi$ result in different ground-state parities. The question mark indicates that ground-state parity is not unique in this region.

transitions appearing solely in the strong-coupling regime are further discussed in the Supplemental Material [46] (Figs. S2, S10, and S11). They are beyond the scope of this manuscript and motivate future works incorporating superconducting quantum interference devices, which could unveil the interesting phase dependence of this regime.

VI. CONCLUSION

In summary, we realized a QD embedded into a Josephson junction with additional side probes revealing neighboring ABSs. These ABSs are shown to be the primary carrier of supercurrent, with measured switching currents matching the predictions of a simple three-site model. This illustrates the crucial role of controlling and detecting localized ABSs in semiconductor-superconductor hybrid devices. Furthermore, by tuning couplings and ABSs, we have demonstrated that the system effectively behaves as an Andreev trimer, whose charging diagram can be fully characterized via either supercurrent or normal probe measurements. This additionally exemplifies how ABS tuning can be done via supercurrent in long-nanowire-based Kitaev chains, for which the normal probes would be farther away from central ABSs [61–63]. Besides that, our study sets the ground for future works on Josephson-junction devices with increased complexity, including longer Andreev molecules predicted to modulate the supercurrent nonlocally [64] and complex Andreev spin qubit devices [25].

ACKNOWLEDGMENTS

This work has been supported by the Dutch Organization for Scientific Research and Microsoft Corporation Station Q. We wish to acknowledge Isidora Araya Day, Anton Akhmerov, Francesco Zatelli, and Jens Paaske for useful discussions and Ghada Badawy and Sasa Gazibegovic for the nanowire growth. G. S. and A. L. Y. acknowledge EU through FET-Open project ANDQC and Spanish AEI through Grant No. TED2021-130292B-C43.

A. B., F. J. B. E., and G. O. S. contributed equally to this work. A. B., J. C. W., and D. v. D. fabricated the device. G. O. S. and A. L. Y. developed the theoretical model and performed numerical simulations. F. J. B. E. and A. B. performed the electrical measurements with help from G. P. M. and N. v. L. A. B. and T. D. designed the experiment. E. P. A. M. B. provided the nanowires. L. P. K. supervised the project. A. B., F. J. B. E., G. O. S., A. L. Y., and L. P. K. prepared the manuscript with input from all authors

DATA AVAILABILITY

All raw data in the publication and the analysis code used to generate figures are publicly available [65]. For every dataset, the exp_name attribute reports the corresponding gate settings.

[1] L. P. Kouwenhoven, D. G. Austing, and S. Tarucha, *Few-electron quantum dots*, Rep. Prog. Phys. **64**, 701 (2001).
[2] W. Lu, Z. Ji, L. Pfeiffer, K. W. West, and A. J. Rimberg, *Real-time detection of electron tunnelling in a quantum dot*, Nature (London) **423**, 422 (2003).
[3] S. Zhu, Y. Song, X. Zhao, J. Shao, J. Zhang, and B. Yang, *The photoluminescence mechanism in carbon dots (graphene quantum dots, carbon nanodots, and polymer dots): Current state and future perspective*, Nano Res. **8**, 355 (2015).
[4] P. Michler, A. Kiraz, C. Becher, W. V. Schoenfeld, P. M. Petroff, L. Zhang, E. Hu, and A. Imamoglu, *A quantum dot single-photon turnstile device*, Science **290**, 2282 (2000).

[5] F. P. García de Arquer, D. V. Talapin, V. I. Klimov, Y. Arakawa, M. Bayer, and E. H. Sargent, *Semiconductor quantum dots: Technological progress and future challenges*, Science **373**, eaaz8541 (2021).

[6] R. Hanson, L. P. Kouwenhoven, J. R. Petta, S. Tarucha, and L. M. K. Vandersypen, *Spins in few-electron quantum dots*, Rev. Mod. Phys. **79**, 1217 (2007).

[7] G. Burkard, T. D. Ladd, A. Pan, J. M. Nichol, and J. R. Petta, *Semiconductor spin qubits*, Rev. Mod. Phys. **95**, 025003 (2023).

[8] M. Tinkham, *Introduction to Superconductivity* (Dover Publications, Inc., Mineola, 2004).

[9] J. Clarke and F. K. Wilhelm, *Superconducting quantum bits*, Nature (London) **453**, 1031 (2008).

[10] M. Kjaergaard, M. E. Schwartz, J. Braumüller, P. Krantz, J. I.-J. Wang, S. Gustavsson, and W. D. Oliver, *Superconducting qubits: Current state of play*, Annu. Rev. Condens. Matter Phys. **11**, 369 (2020).

[11] F. Ando, Y. Miyasaka, T. Li, J. Ishizuka, T. Arakawa, Y. Shiota, T. Moriyama, Y. Yanase, and T. Ono, *Observation of superconducting diode effect*, Nature (London) **584**, 373 (2020).

[12] P. Jarillo-Herrero, J. A. van Dam, and L. P. Kouwenhoven, *Quantum supercurrent transistors in carbon nanotubes*, Nature (London) **439**, 953 (2006).

[13] J. A. van Dam, Y. V. Nazarov, E. P. A. M. Bakkers, S. De Franceschi, and L. P. Kouwenhoven, *Supercurrent reversal in quantum dots*, Nature (London) **442**, 667 (2006).

[14] H. I. Jørgensen, T. Novotný, K. Grove-Rasmussen, K. Flensberg, and P. E. Lindelof, *Critical current* 0-π *transition in designed Josephson quantum dot junctions*, Nano Lett. **7**, 2441 (2007).

[15] G. Katsaros, P. Spathis, M. Stoffel, F. Fournel, M. Mongillo, V. Bouchiat, F. Lefloch, A. Rastelli, O. G. Schmidt, and S. De Franceschi, *Hybrid superconductor–semiconductor devices made from self-assembled SiGe nanocrystals on silicon*, Nat. Nanotechnol. **5**, 458 (2010).

[16] D. B. Szombati, S. Nadj-Perge, D. Car, S. R. Plissard, E. P. A. M. Bakkers, and L. P. Kouwenhoven, *Josephson* ϕ_0*-junction in nanowire quantum dots*, Nat. Phys. **12**, 568 (2016).

[17] A. Bargerbos, M. Pita-Vidal, R. Žitko, J. Ávila, L. J. Splitthoff, L. Grünhaupt, J. J. Wesdorp, C. K. Andersen, Y. Liu, L. P. Kouwenhoven, R. Aguado, A. Kou, and B. van Heck, *Singlet-doublet transitions of a quantum dot Josephson junction detected in a transmon circuit*, PRX Quantum **3**, 030311 (2022).

[18] A. Bargerbos, M. Pita-Vidal, R. Žitko, L. J. Splitthoff, L. Grünhaupt, J. J. Wesdorp, Y. Liu, L. P. Kouwenhoven, R. Aguado, C. K. Andersen, A. Kou, and B. van Heck, *Spectroscopy of spin-split Andreev levels in a quantum dot with superconducting leads*, Phys. Rev. Lett. **131**, 097001 (2023).

[19] R. Maurand, T. Meng, E. Bonet, S. Florens, L. Marty, and W. Wernsdorfer, *First-order* 0-π *quantum phase transition in the Kondo regime of a superconducting carbon-nanotube quantum dot*, Phys. Rev. X **2**, 011009 (2012).

[20] E. J. H. Lee, X. Jiang, R. Aguado, G. Katsaros, C. M. Lieber, and S. De Franceschi, *Zero-bias anomaly in a nanowire quantum dot coupled to superconductors*, Phys. Rev. Lett. **109**, 186802 (2012).

[21] J.-D. Pillet, P. Joyez, R. Žitko, and M. F. Goffman, *Tunneling spectroscopy of a single quantum dot coupled to a superconductor: From Kondo ridge to Andreev bound states*, Phys. Rev. B **88**, 045101 (2013).

[22] A. Jellinggaard, K. Grove-Rasmussen, M. H. Madsen, and J. Nygård, *Tuning Yu-Shiba-Rusinov states in a quantum dot*, Phys. Rev. B **94**, 064520 (2016).

[23] C. Padurariu and Y. V. Nazarov, *Theoretical proposal for superconducting spin qubits*, Phys. Rev. B **81**, 144519 (2010).

[24] M. Hays, V. Fatemi, D. Bouman, J. Cerrillo, S. Diamond, K. Serniak, T. Connolly, P. Krogstrup, J. Nygård, A. Levy Yeyati, A. Geresdi, and M. H. Devoret, *Coherent manipulation of an Andreev spin qubit*, Science **373**, 430 (2021).

[25] M. Pita-Vidal, A. Bargerbos, R. Žitko, L. J. Splitthoff, L. Grünhaupt, J. J. Wesdorp, Y. Liu, L. P. Kouwenhoven, R. Aguado, B. van Heck, A. Kou, and C. K. Andersen, *Direct manipulation of a superconducting spin qubit strongly coupled to a transmon qubit*, Nat. Phys. **19**, 1110 (2023).

[26] M. Pita-Vidal, J. J. Wesdorp, L. J. Splitthoff, A. Bargerbos, Y. Liu, L. P. Kouwenhoven, and C. K. Andersen, *Strong tunable coupling between two distant superconducting spin qubits*, Nat. Phys. **20**, 1158 (2024).

[27] T. Dvir, G. Wang, N. van Loo, C.-X. Liu, G. P. Mazur, A. Bordin, S. L. D. ten Haaf, J.-Y. Wang, D. van Driel, F. Zatelli, X. Li, F. K. Malinowski, S. Gazibegovic, G. Badawy, E. P. A. M. Bakkers, M. Wimmer, and L. P. Kouwenhoven, *Realization of a minimal Kitaev chain in coupled quantum dots*, Nature (London) **614**, 445 (2023).

[28] A. Tsintzis, R. S. Souto, and M. Leijnse, *Creating and detecting poor man's Majorana bound states in interacting quantum dots*, Phys. Rev. B **106**, L201404 (2022).

[29] S. L. D. ten Haaf, Q. Wang, A. M. Bozkurt, C.-X. Liu, I. Kulesh, P. Kim, D. Xiao, C. Thomas, M. J. Manfra, T. Dvir, M. Wimmer, and S. Goswami, *A two-site Kitaev chain in a two-dimensional electron gas*, Nature (London) **630**, 329 (2024).

[30] R. S. Deacon, A. Oiwa, J. Sailer, S. Baba, Y. Kanai, K. Shibata, K. Hirakawa, and S. Tarucha, *Cooper pair splitting in parallel quantum dot Josephson junctions*, Nat. Commun. **6**, 7446 (2015).

[31] B. Probst, F. Domínguez, A. Schroer, A. L. Yeyati, and P. Recher, *Signatures of nonlocal Cooper-pair transport and of a singlet-triplet transition in the critical current of a double-quantum-dot Josephson junction*, Phys. Rev. B **94**, 155445 (2016).

[32] D. Bouman, R. J. J. van Gulik, G. Steffensen, D. Pataki, P. Boross, P. Krogstrup, J. Nygård, J. Paaske, A. Pályi, and A. Geresdi, *Triplet-blockaded Josephson supercurrent in double quantum dots*, Phys. Rev. B **102**, 220505(R) (2020).

[33] J. C. Estrada Saldaña, A. Vekris, R. Žitko, G. Steffensen, P. Krogstrup, J. Paaske, K. Grove-Rasmussen, and J. Nygård, *Two-impurity Yu-Shiba-Rusinov states in coupled quantum dots*, Phys. Rev. B **102**, 195143 (2020).

[34] O. Kürtössy, Z. Scherübl, G. Fülöp, I. E. Lukács, T. Kanne, J. Nygård, P. Makk, and S. Csonka, *Andreev molecule in parallel InAs nanowires*, Nano Lett. **21**, 7929 (2021).

[35] M. Coraiola, D. Z. Haxell, D. Sabonis, M. Hinderling, S. C. ten Kate, E. Cheah, F. Krizek, R. Schott, W. Wegscheider, and F. Nichele, *Spin-degeneracy breaking and parity*

transitions in three-terminal Josephson junctions, Phys. Rev. X **14**, 031024 (2024).

[36] H. Pan and S. Das Sarma, *Physical mechanisms for zero-bias conductance peaks in Majorana nanowires*, Phys. Rev. Res. **2**, 013377 (2020).

[37] E. Prada, P. San-Jose, M. W. A. de Moor, A. Geresdi, E. J. H. Lee, J. Klinovaja, D. Loss, J. Nygård, R. Aguado, and L. P. Kouwenhoven, *From Andreev to Majorana bound states in hybrid superconductor–semiconductor nanowires*, Nat. Rev. Phys. **2**, 575 (2020).

[38] M. Valentini, F. Peñaranda, A. Hofmann, M. Brauns, R. Hauschild, P. Krogstrup, P. San-Jose, E. Prada, R. Aguado, and G. Katsaros, *Nontopological zero-bias peaks in full-shell nanowires induced by flux-tunable Andreev states*, Science **373**, 82 (2021).

[39] C.-X. Liu, G. Wang, T. Dvir, and M. Wimmer, *Tunable superconducting coupling of quantum dots via Andreev bound states in semiconductor-superconductor nanowires*, Phys. Rev. Lett. **129**, 267701 (2022).

[40] A. Bordin, G. Wang, C.-X. Liu, S. L. D. ten Haaf, N. van Loo, G. P. Mazur, D. Xu, D. van Driel, F. Zatelli, S. Gazibegovic, G. Badawy, E. P. A. M. Bakkers, M. Wimmer, L. P. Kouwenhoven, and T. Dvir, *Tunable crossed Andreev reflection and elastic cotunneling in hybrid nanowires*, Phys. Rev. X **13**, 031031 (2023).

[41] F. Zatelli, D. van Driel, D. Xu, G. Wang, C.-X. Liu, A. Bordin, B. Roovers, G. P. Mazur, N. van Loo, J. C. Wolff, A. M. Bozkurt, G. Badawy, S. Gazibegovic, E. P. A. M. Bakkers, M. Wimmer, L. P. Kouwenhoven, and T. Dvir, *Robust poor man's Majorana zero modes using Yu-Shiba-Rusinov states*, Nat. Commun. **15**, 7933 (2024).

[42] C.-X. Liu, A. M. Bozkurt, F. Zatelli, S. L. D. ten Haaf, T. Dvir, and M. Wimmer, *Enhancing the excitation gap of a quantum-dot-based Kitaev chain*, Commun. Phys. **7**, 235 (2024).

[43] J. C. Estrada Saldaña, A. Vekris, G. Steffensen, R. Žitko, P. Krogstrup, J. Paaske, K. Grove-Rasmussen, and J. Nygård, *Supercurrent in a double quantum dot*, Phys. Rev. Lett. **121**, 257701 (2018).

[44] S. Heedt, M. Quintero-Pérez, F. Borsoi, A. Fursina, N. van Loo, G. P. Mazur, M. P. Nowak, M. Ammerlaan, K. Li, S. Korneychuk, J. Shen, M. A. Y. van de Poll, G. Badawy, S. Gazibegovic, N. de Jong, P. Aseev, K. van Hoogdalem, E. P. A. M. Bakkers, and L. P. Kouwenhoven, *Shadow-wall lithography of ballistic superconductor–semiconductor quantum devices*, Nat. Commun. **12**, 4914 (2021).

[45] A. Bordin, X. Li, D. van Driel, J. C. Wolff, Q. Wang, S. L. D. ten Haaf, G. Wang, N. van Loo, L. P. Kouwenhoven, and T. Dvir, *Crossed Andreev reflection and elastic cotunneling in three quantum dots coupled by superconductors*, Phys. Rev. Lett. **132**, 056602 (2024).

[46] See Supplemental Material at http://link.aps.org/supplemental/10.1103/PhysRevX.15.011046 for a deeper discussion of the model, nanofabrication and circuit details, measurement procedures, and extended data, which includes Refs. [8,13,43–45,47–53].

[47] T. Novotný, A. Rossini, and K. Flensberg, *Josephson current through a molecular transistor in a dissipative environment*, Phys. Rev. B **72**, 224502 (2005).

[48] I. Araya Day, S. Miles, D. Varjasand, and A. R. Akhmerov, *Pymablock*, Zenodo (2023), 10.5281/zenodo.7995684.

[49] I. Araya Day, S. Miles, H. K. Kerstens, D. Varjas, and A. R. Akhmerov, *Pymablock: An algorithm and a package for quasi-degenerate perturbation theory*, SciPost Phys. Codebases 50 (2025).

[50] F. Domínguez and A. L. Yeyati, *Quantum interference in a Cooper pair splitter: The three sites model*, Physica (Amsterdam) **75E**, 322 (2016).

[51] S. De Franceschi, L. Kouwenhoven, C. Schönenberger, and W. Wernsdorfer, *Hybrid superconductor–quantum dot devices*, Nat. Nanotechnol. **5**, 703 (2010).

[52] N. van Loo, G. P. Mazur, T. Dvir, G. Wang, R. C. Dekker, J.-Y. Wang, M. Lemang, C. Sfiligoj, A. Bordin, D. van Driel, G. Badawy, S. Gazibegovic, E. P. A. M. Bakkers, and L. P. Kouwenhoven, *Electrostatic control of the proximity effect in the bulk of semiconductor-superconductor hybrids*, Nat. Commun. **14**, 3325 (2023).

[53] J. Bauer, A. Oguri, and A. C. Hewson, *Spectral properties of locally correlated electrons in a Bardeen–Cooper–Schrieffer superconductor*, J. Phys. Condens. Matter **19**, 486211 (2007).

[54] E. J. H. Lee, X. Jiang, M. Houzet, R. Aguado, C. M. Lieber, and S. De Franceschi, *Spin-resolved Andreev levels and parity crossings in hybrid superconductor–semiconductor nanostructures*, Nat. Nanotechnol. **9**, 79 (2013).

[55] A. Martín-Rodero and A. Levy Yeyati, *Josephson and Andreev transport through quantum dots*, Adv. Phys. **60**, 899 (2011).

[56] F. Bennebroek Evertsz', *Supercurrent modulation by Andreev bound states in a quantum dot Josephson junction*, Master's thesis, Delft University of Technology, 2023.

[57] V. Meden, *The Anderson–Josephson quantum dot—A theory perspective*, J. Phys. Condens. Matter **31**, 163001 (2019).

[58] K. Grove-Rasmussen, G. Steffensen, A. Jellinggaard, M. H. Madsen, R. Žitko, J. Paaske, and J. Nygård, *Yu–Shiba–Rusinov screening of spins in double quantum dots*, Nat. Commun. **9**, 2376 (2018).

[59] A. V. Rozhkov and D. P. Arovas, *Josephson coupling through a magnetic impurity*, Phys. Rev. Lett. **82**, 2788 (1999).

[60] L. Pavešić, R. Aguado, and R. Žitko, *Strong-coupling theory of quantum-dot Josephson junctions: Role of a residual quasiparticle*, Phys. Rev. B **109**, 125131 (2024).

[61] A. Tsintzis, R. S. Souto, K. Flensberg, J. Danon, and M. Leijnse, *Majorana qubits and non-Abelian physics in quantum dot–based minimal Kitaev chains*, PRX Quantum **5**, 010323 (2024).

[62] S. Miles, D. van Driel, M. Wimmer, and C.-X. Liu, *Kitaev chain in an alternating quantum dot-Andreev bound state array*, Phys. Rev. B **110**, 024520 (2024).

[63] A. Bordin, C.-X. Liu, T. Dvir, F. Zatelli, S. L. D. t. Haaf, D. van Driel, G. Wang, N. van Loo, T. van Caekenberghe, J. C. Wolff, Y. Zhang, G. Badawy, S. Gazibegovic, E. P. A. M. Bakkers, M. Wimmer, L. P. Kouwenhoven, and G. P. Mazur, *Signatures of Majorana protection in a three-site Kitaev chain*, arXiv:2402.19382.

[64] M. Kocsis, Z. Scherübl, G. Fülöp, P. Makk, and S. Csonka, *Strong nonlocal tuning of the current-phase relation of a quantum dot based Andreev molecule*, Phys. Rev. B **109**, 245133 (2024).

[65] A. Bordin, F. J. Bennebroek Evertsz', and G. O. Steffensen, *Impact of Andreev bound states within the leads of a quantum dot Josephson junction*, Zenodo (2025), 10.5281/zenodo.14826592.